Romanian Reports in Physics, Vol. 67, No. 4, P. 1512–1524, 2015

Dedicated to
International Year of Light 2015

IN VITRO EVALUATION OF THE MORPHOLOGICAL AND BIOCHEMICAL CHANGES INDUCED BY Si/SiO_2 QD_S EXPOSURE OF HepG2 CELLS

L. STANCA[1,2], C. SIMA[3], S.N. PETRACHE (VOICU) [2,4], A.I. SERBAN [1], A. DINISCHIOTU[2]

[1] University of Agronomical Sciences and Veterinary Medicine Bucharest, Faculty of Veterinary Medicine, Department of Preclinical Sciences, 105 Splaiul Independentei, postal code 050097, district 5, Bucharest, Romania, E-mails: lory_stanca@yahoo.com, irensro@yahoo.com
[2] University of Bucharest, Faculty of Biology, Department of Biochemistry and Molecular Biology, 91–95 Splaiul Independentei, postal code 050095, district 5, Bucharest, Romania, E-mails: lory_stanca@yahoo.com, ancadinischiotu@yahoo.com, sori.petrache@yahoo.com
[3] National Institute of Laser, Plasma and Radiation Physics, Laser Department, 409 Atomistilor St., Bucharest-Magurele, postal code 077125, Romania, E-mail: cornelia.sima@inflpr.ro
[4] "Vasile Goldis" Western University of Arad, Institute of Life Sciences, Department of Experimental and Applied Biology, 86 Rebreanu St., Arad 310414, Romania; E-mail: sori.petrache@yahoo.com

Received October 7, 2015

Abstract. Heavy metal based QDs are promising bioimaging tools, although some toxicity related concerns exist. Thus, we manufactured by pulsed laser ablation method Si/SiO_2 QDs, with low elemental toxicity. They were 5 nm in diameter, with a crystalline silicon core and a 1.5 nm amorphous SiO_2 layer, and exhibited a fluorescence peak at ~690 nm under 325 nm excitation wavelength. We exposed HepG2 cells to 25–300 μg/ml QDs for up to 72 h and evaluated reactive oxygen species, cells viability, cytoskeleton architecture, cell morphology and integrity. Our results indicate HepG2 cells tolerate high doses of Si/SiO_2 QDs, without suffering significant damage.

Key words: silicon QDs, HepG2, nanotoxicity, actin cytoskeleton, oxidative stress, Nrf2.

1. INTRODUCTION

In the past few years, quantum dots (QDs) have become the subject of numerous research focused on their synthesis, solubilisation and bio-functionalization. The nanotechnology industry has known a very rapid development, both regarding the development of existing applications and the discovery of new ones [1–2]. Although QDs are in many respects more performant compared to protein fluorescent markers [3–4], there are still numerous issues associated with their use, thus their great potential in bio-imaging remains incompletely exploited, mainly due to the toxicological concerns [5–6]. Current approaches to reduce QDs toxicity often include the encapsulation in a SiO_2 shell

[7–8], therefore the motivation for our present study, aimed the *in vitro* characterization of Si/SiO_2 QDs biocompatibility. The benefits of silicon, as: low elemental toxicity, potential biodegradability, great abundance and reduced costs, promote Si QDs as good candidates to replace cadmium dots for *in vivo* applications [9–10]. Tissue imaging using far-red or NIR wavelengths could help overcome the tissue autofluorescence issues, improve tissue penetration and reduce the absorption of the major interfering molecules *(e.g.* hemoglobin and water) [11].

Due to the special physicochemical properties at the nanoscale level, all nanomaterials, including amorphous silica raise toxicity concerns [12–13]. Silicon nanoparticle exposure was shown to reduce proliferation in myocardial cells, human renal embryonic cells and hepatocyte cell lines [14–16]. *In vitro* studies have shown that nanoparticle exposure can induce oxidative stress, apoptosis, and cytokine expression [17]. In the present study, we have aimed at testing these hypotheses for the case of Si/SiO_2 QDs, considering that their small size (even when compared to nanoparticles $\leq$ 100 nm) could play a deterministic role in their toxicity.

2. MATERIALS AND METHODS

2.1. QDS PREPARATION AND CHARACTERIZATION

The manufacturing process of the silicon QDs was described in detail previously [18]. The particles were spherical, 98.8% were smaller than 10 nm in diameter, and the peak of the log-normal distribution was at 4 nm. The particles core was composed of crystalline silicon, surrounded by an amorphous SiO_2 layer, about 1.5 nm thick [19]. When excited with a 325 nm wavelength radiation, the Si/SiO_2 QDs had a wide emission spectrum, ranging from 400 to 800 nm, with a maximum at ~ 1.8 eV, causing a red fluorescence – and a smaller peak at 2.4–2.6 eV. The 1.8 eV emission was attributed to the quantum confinement mechanism, and was generated due to the small size of the crystalline Si core of the QDs. After the oxidation of the particles this fluorescence was diminished, and the particle surface was considered completely oxidized [20].

2.2. QDS PREPARATION FOR CELL TREATMENTS

Bulk Si/SiO_2 nanopowder was weighed, suspended in sterile PBS (10 mM PO_4^{3-}, 137 mM NaCl, and 2.7 mM KCl), and thoroughly homogenised by 15 minutes (min.) ultrasonication (UP50H–Compact Lab Homogenizer-Hielscher Ultrasonics GmbH), on ice. The process was repeated for five consecutive days.

Then the suspension was allowed to settle, in a cool dark place, for 30 days, the suspension was carefully collected, and the remaining sediment was completely dried and weighed. The remaining suspended particle concentration was 0.0015 g/ml. The suspension was sterilised (120 °C, 3 × 20 min.) and before adding it to the cell cultures, the suspension was always homogenized by ultra-sonication.

2.3. VISUALIZATION OF THE Si/SiO2 QDS AT THE FLUORESCENCE MICROSCOPE

A volume of 20 µl QDs suspension was placed on a glass slide and allowed to dry. The red fluorescence of the QDs was visible directly in the microscope's ocular (Olympus IX71, Hg fluorescence lamp, standard filter set with three band excitation DAPI/FITC/TRITC, Colorview II digital camera). The images background was corrected using the Cell^F imaging software (Olympus, Athens, Greece).

2.4. CELL CULTURE AND CELL TREATMENTS

The HepG2 cell line (ATCC HB-8065) is an adherent hepatic carcinoma cell line, with epithelial morphology. The cells were grown in MEM medium, pH 7.4, 2 mM L-glutamine, supplemented with 1 mM sodium pyruvate, 1.5 g/l sodium carbonate, 1 % antibiotic-antimycotic mix and 10 % foetal bovine serum (FBS) and maintained at 37°C, in an atmosphere with 95 % humidity and 5 % CO_2. The cells were exposed for 6, 12, 24, 48 and 72 h to 25, 100, 200 or 300 µg QDs/ml. For controls, we added a volume of sterile PBS in the growth medium, corresponding to the volume of QDs suspension added for each QDs dose.

2.5. THE CELL LYSATE PREPARATION

After the exposure intervals, the medium containing the QDs was removed, the cells were detached by 0.025 % trypsin solution and were centrifuged (1500 rpm, 18°C, 10 min.). Then the cells were re-suspended in PBS, sonicated (3 times, 30 seconds, on ice) and centrifuged at 3000 rpm, 10 min., at 4 °C. The supernatant was aliquoted and frozen at –80 °C, for subsequent biochemical and immunochemical analysis.

2.6. PROTEIN CONCENTRATION ASSESSMENT

Protein concentration was determined according to the Bradford method [21] using bovine serum albumin as standard.

2.7. INTRACELLULAR SUPEROXIDE ANION QUANTIFICATION

After the cells were exposed to the desired QDs concentrations, were detached from the culture flasks, centrifuged (1500 rpm, 5 min., 18°C), and counted. Then, they were gently re-suspended in growth medium (without bovine foetal serum) with 0.5 mg/ml nitroblue tetrazolium (NBT), incubated at 37°C for one hour. Then, the cells were centrifuged again (1500 rpm, 5 min., 18°C) and the pellet was solubilised in 200 µl DMSO, and sonicated for 30 seconds. The optical density of blue formazan, generated by the reduction of NBT by superoxide, was read at 520 nm. The results were reported to their corresponding controls.

2.8. CELL INTEGRITY ASSESSMENT

Extracellular lactate dehydrogenase (LDH) was quantified using the commercial kit (*in vitro* Toxicology Assay Kit – Lactic Dehydrogenase, Sigma-Aldrich, St. Louis, MO, USA), according to the manufacturer's instructions. After treatments, the media were collected, centrifuged (5 000 rpm, 10 min., 18°C), and the cell-free supernatants were used for assay. For the assays blank we used media with 10% FBS, which were kept in the incubator, in a cell free-flask, for 6, 12 and 24 hours.

2.9. THE CELL PROLIFERATION AND VIABILITY TEST MTT

The MTT assay is using the 3-(4,5-dimethilthiazol-2-il)-2,5-dipheniltetrazolium bromide (MTT), a yellow coloured substance, which can penetrate the cell membrane. Once inside the cell, the compound is reduced under the activity of the NAD(P)H-dependent mitochondrial succinate dehydrogenases to a purple insoluble formazan salt [22]. HepG2 cells were exposed to 25, 50, 100, 200 and 300 µg/ml QDs for 24, 48 and 72 h. At the end of each QDs exposure interval, the cell medium was replaced with PBS containing 1 mg/ml MTT and incubated at 37°C for 2 hours. Then, the formazan crystals were solubilized in 2-propanol and the absorbance was read at 595 nm. The absorbance of samples exposed to QDs was reported to the corresponding time-interval controls.

Based on the MTT data, a Hill-type equation (1) was used to fit a dose response curve, in order to determine the IC50 dose.

$$y = \text{START} + (\text{END} - \text{START})\frac{x^n}{k^n + x^n}, \tag{1}$$

where y represents viability; START represents viability of the control cells; END is the minimum viability obtained for the analysed time interval; x represents the QDs concentration applied; n is the Hill coefficient; k is the IC50.

2.10. WESTERN BLOTTING

The total protein extracts were denatured (95°C, 5 min.) and were resolved by SDS-PAGE (30 µg/well). The separating gel contained 15% polyacrylamide, in 0.375 M Tris-HCl, pH 8.8, 0.1% SDS, 3.3×10^{-4} % ammonium persulfate; $6.6 \times \times 10^{-4}$ % TEMED, while the stacking gel contained 4.5 % polyacrylamide in 0.125 M Tris-HCl, pH 6.8, 0.1% SDS, 5×10^{-4} % ammonium persulfate, 0.001 % TEMED. The gels were run at constant voltage (90 V) at room temperature (RT). The resolved proteins were transferred onto PVDF membranes using the wet transfer method (25 mM Tris, 192 mM glycin, 20 % methanol) at 350 mA, 3 ¾ h at 4°C. Then the membranes were incubated over night with the interest primary antibodies: Cu/Zn-SOD (SOD-1(G11) sc-17767, Santa Cruz Biotechnology, Inc., Dallas, TX, USA), Nrf2 (H-300 SC-13032, Santa Cruz Biotechnology, Inc., Dallas, TX, USA) and the house-keeping protein ß-actin (A1978, Sigma-Aldrich, St. Louis, MO, USA). The immunoreactive bands were developed using the Western Breeze Chromogenic Immunodetection System (Invitrogen, Carlsbad, CA, USA) according to the instructions, and digitalised using the Vilbert Lourmat and densitometrated using the ImageJ software.

2.11. FLUORESCENT STAINING OF THE CYTOSKELETON AND NUCLEI

Intracellular accumulation of nanoparticles and QDs aggregates can alter the cellular internal architecture, and it might perturb the actin cytoskeleton. In order to assess if these changes occur in HepG2 cells exposed to 25 and 100 µg/ml QDs for 24 h, we stained the actin cytoskeleton using fluorescein isothiocianate (FITC) coupled with phallioidin. After 24 h of exposure to 25 or 100 µg/ml QDs, the cells grown on glass coverslips were gently washed with PBS. The cells were permeabilized with 70 % methanol, 15 min., at RT) with 10 µg/mL phalloidin/FITC (in PBS, 1.2 % BSA). To stain the nuclei, the cells were washed three times with PBS, and incubated 15 min. with 2 µg/mL DAPI (in PBS), at RT. The coverslips were fixed on glass slides with mounting medium (ProLong Gold Antifade Reagent, Invitrogen, Carlsbad, CA, USA), dried, and visualised at the fluorescence microscope (Olympus IX71, Cell F software).

2.12. QUANTITATION OF INFLAMMATORY CYTOKINES

The extracellular and intracellular levels of IL-2, IL-4, IL-6, IL-8, IL-10, GM-CSF, IFN-γ and TNF-α cytokines were evaluated using a cytokine multiplex assay (Bio-Plex Pro Human Cytokine 8-plex, Bio-Rad Laboratories, Hercules, CA, USA). Cell lysates had a total protein concentration of 800 µg/ml and the conditioned media samples had 600 µg/ml. The cytokine expression level was analyzed using the Bio-Plex MAGPIX System (Bio-Rad Laboratories, Hercules,

CA, USA), and concentrations of each cytokine were determined using Bio-Plex Manager software version 6.0 (Bio-Rad Laboratories, Hercules, CA, USA). Only IL-8 concentration was in the range of the kit.

3. RESULTS AND DISCUSSIONS

3.1. THE EFFECTS OF HepG2 CELLS EXPOSURE TO Si/SiO_2 QDs ON CELL VIABILITY

Our attempt in describing a toxicological mechanism activated by Si/SiO_2 QDs exposure employed an *in vitro* model, in order to reduce the number of variable parameters (which might hinder the elucidation of toxicological mechanisms in complex *in vivo* experimental models). HepG2 cells are routinely used in many toxicology studies, for monitoring cytotoxic and genotoxic compounds, for evaluating chemo-protective compounds, and also for assessing hepatocyte specific modifications and the specific biochemical mechanisms activated by these substances. Although these cells are transformed, they retain numerous characteristics of the normal human hepatocyte, thus, they are often used as experimental models.

The viability of HepG2 was affected by QDs exposure, in a time and dose dependent manner (Fig. 1). For the 24 h exposure interval, the IC50 dose was 111 μg/ml QDs and for the 48 h interval the IC50 dose was 57 μg/ml QDs.

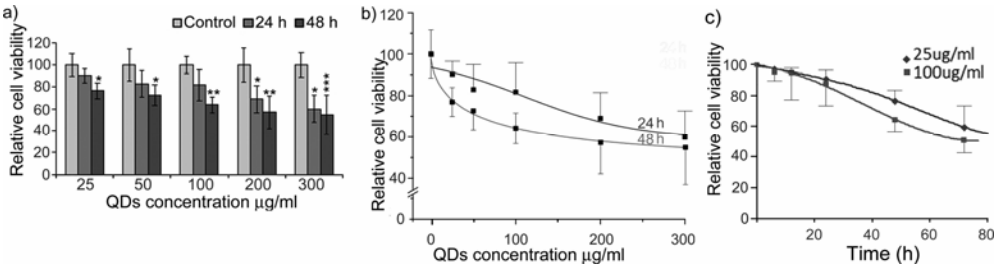

Fig. 1 – The effects of HepG2 exposure to Si/SiO_2 QDs on cell viability: a) the MTT test for QDs doses from 25 to 300 μg/ml, applied for 24 and 48 h. The statistically significant changes (Student's t test) are indicated *$p < 0.05$; **$p < 0.01$; ***$p < 0.001$; b) dose response curve based on the data in a); c) the effects of the 25 or 100 μg/ml QDs doses for up to 72 h (the trendlines are described by polynomial functions). All data are relative to controls, and the relative standard deviation (RSD) is given.

Using this information, we chose the doses of 100 μg/ml (an approximate of the IC50 dose for 24 h) and 25 μg/ml for subsequent analysis. The effect on cell viability of these doses was subsequently tested for up to 72 h (Fig. 1c). The data revealed that a 12 h exposure to 100 μg/ml Si/SiO_2 QDs did not affect cellular viability, which began to diminish starting with the 24 h interval. After 72 h of QDs exposure, both 25 and 100 μg/ml Si/SiO_2 QDs doses significantly diminished

the viability, by 40 % and 50 % respectively. Moreover, the trend lines (Fig. 1c) seem to suggest that longer exposure intervals would not induce viability or cell proliferation decreases greater than the 50 % threshold.

3.2. QDS INDUCED CHANGES THEY INDUCED AT CYTOSKELETAL AND NUCLEAR LEVELS IN HepG2 CELLS

The QDs fluorescence was visualised without the cells (Fig. 2) and also in HepG2 cell cultures, at both the 25 and 100 μg/ml doses applied for 24 h (Fig. 3). The fluorescence of QDs dried residue was strong, observable directly in the microscope ocular. The PBS solution in which the QDs were suspended had no fluorescence, in the same conditions (Fig. 2c).

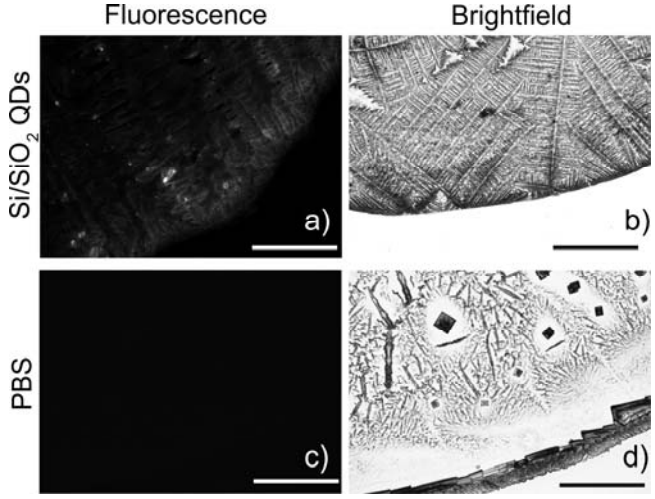

Fig. 2 – QDs characteristic fluorescence in a) as observed using the Olympus IX71 inverted microscope, with a Hg lamp and a standard filter with three excitation bands DAPI/FITC/TRITC and a Colorview II camera. The QDs brightfield micrographs are shown in b) and the PBS one is shown in d). In c) the PBS dry residue had no fluorescence in the same experimental conditions. Bar represents 200 μm.

In the presence of HepG2 cells (Fig. 3) although QDs seems to cover uniformly the surface of the culture dish (Fig. 3a,c) forming small clusters, the characteristic fluorescence was observed only in cell populated areas, suggesting there QDs might aggregate in larger clusters, whose fluorescence would be detectable by our imaging system. The 25 and 100 μg/ml QDs concentrations, used by us, were probably not high enough to provide a strong fluorescence emission, as it was seen in the case of the dried QDs residue shown in Fig. 2. We couldn't establish if QDs aggregates penetrated the cells, although they seemed to have pericellular localization (Fig. 4e,f). The cytoskeleton has an essential role in

controlling the cell cycle, proliferation and apoptosis. In the control cells, the phalloidin-FITC stain revealed actin stress fibres, as spatially ordered filaments, which surrounded the nuclear regions, and more frequently contoured the cell edges (Fig. 4b). In Si/SiO_2 QDs exposed cells, the actin stress fibres were more diffusely stained and disorganised (Fig. 4f), suggesting the actin cytoskeleton depolymerized. Actin cytoskeleton disorganization is an early phenomenon associated with nanoparticle exposure, and it was shown to be correlated with the inhibition of proliferation and differentiation [23] and cell migration [24]. Cell adherence to the substrate might also be affected by the disorganization of the focal adhesion complexes. A diminished adherence might lead to cell detachment from the substrate and the initiation of pro-apoptotic signalling pathways. This hypothesis was tested by observing the nuclei morphology. After 24 h of exposure to 100 μg/ml QDs condensed chromatin and pyknotic nuclei were observed, while other nuclei underwent karyorrhexis (Fig. 4g), indicating apoptosis. These microscopic observations were probably not enough to explain the reduced values of the MTT test. Moreover, despite the apoptosis, we also observed cells actively involved in the division process (Fig. 4g).

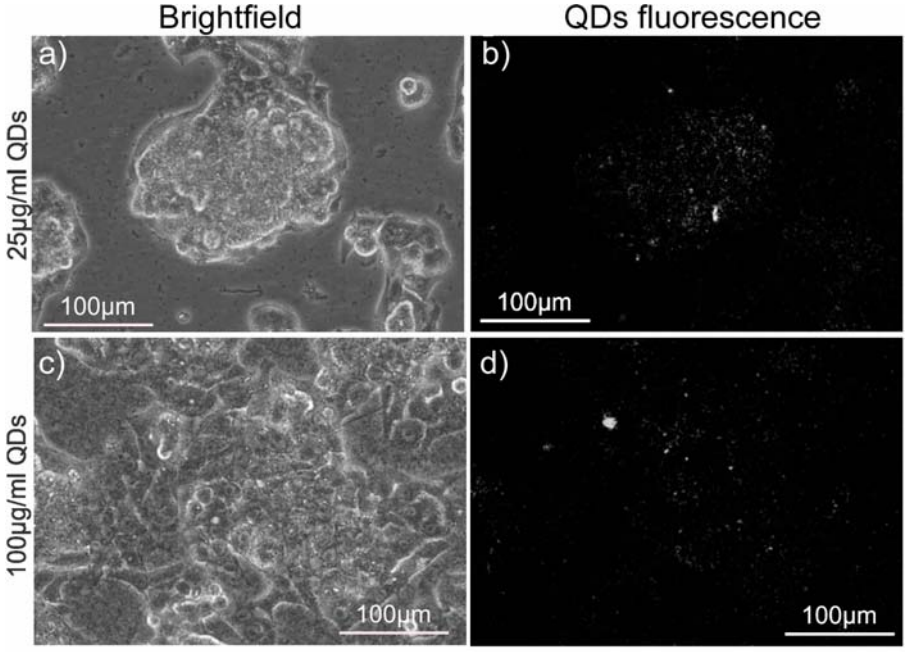

Fig. 3 – Micrographs representing the QDs interaction with the HepG2 cells, and their accumulation in proximity of the cell islands. The cells were exposed to 25 μg/ml (a, b) or 100 μg/ml (c, d) for 24 h and visualised in brightfield (a, c). The same cell fields were observed in fluorescence microscopy. QDs emission was observed in discrete areas, mainly in cell-covered regions of the culture flask, where the dots aggregated. The aquisition time for the fluorescence micrographs was 200 ms. Bar represents 100 μm.

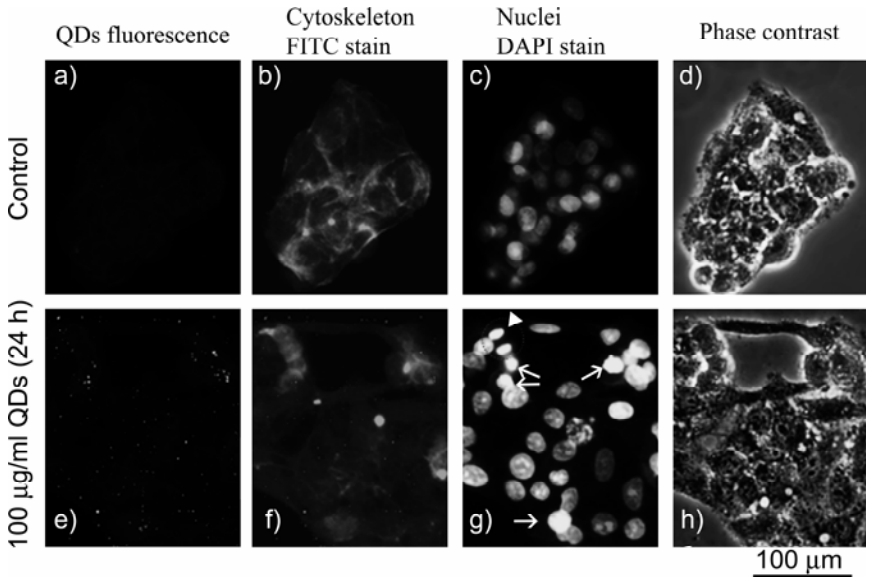

Fig. 4 – Cytoskeletal and nuclear morphology of HepG2 cells exposed to QDs. QDs fluorescence is shown in a) and e). No signal was detected in the control cells a). In QDs exposed cells, QDs fluorescence was detected as small discrete dots, probably due to QDs aggregation in small clusters. Actin cytoskeleton was stained with FITC and shown in b) and f) (images also contain the QDs fluorescent signal). Nuclei (stained with DAPI) morphology is shown in c) and g). After 24 h, in QDs exposed cells chromatin condensed and pyknotic nuclei appeared (arrows), while some nuclei are fragmented (in the centre of (g) panel). Still, some cells are actively involved in division, as indicates the telophase stage observed in g), marked with an arrow head. In the d) and h), phase contrast micrographs are shown. Bar represents 100 µm.

3.3. BIOCHEMICAL CHANGES INDUCED BY Si/SiO_2 QDs IN HepG2 CELLS

The increase of intracellular superoxide anion levels was detected only in the 100 µg/ml QDs exposed cells for 24 h (20.6 % higher than control) (Fig. 5a). This level of superoxide did not affect the cell plasma membrane, as the LDH test indicated (Fig. 5b). This made cell death mechanisms involving cell membrane rupture (e.g. *necrosis*) improbable.

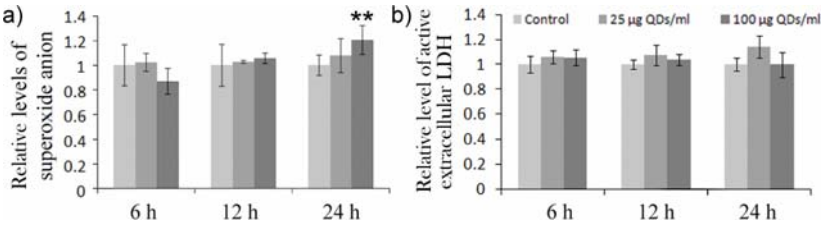

Fig. 5 – The intracellular superoxide anion levels a) and cellular integrity b). Data are shown as relative values (reported to the controls) ± RSD. $^{**}p < 0.01$.

For the onset of oxidative stress, both the increase of reactive oxygen species and the inadequate response of the antioxidant defence mechanisms, especially antioxidant enzymes need to take place. The nanoparticle cytotoxic mechanism was described as the hierarchical oxidative stress model [25–26]. According to this model, when reactive oxygen species are mildly increased (as in our case) the cells should respond by activating the antioxidant mechanisms, which commonly include the activation of the Nrf2 (erythroid 2-related factor 2). Nrf2 holds a key role in the management of oxidative stress, by controlling the expression and coordinated activation of a battery of genes coding for detoxifying enzymes, xenobiotic transporters, anti-apoptotic proteins and proteasome components. Human Nrf2 has a molecular weight of 66 kDa, but, Nrf2 immumoreactive bands were also identified at 98 and 118 kDa [27]. These are the phosphorylated forms of the human endogenous Nrf2, and their presence is associated with oxidative stress. Our immunoblots also revealed the 98 kDa form, and the expected 66 kDa Nrf2 forms (Fig. 6a).

Surprisingly, the expression levels of the phosphorylated Nrf2 was diminished at all the time intervals analysed (6 h, 12 h and 24 h) in HepG2 cells exposed to the 100 µg/ml QDs dose compared to controls. The densitometric analysis revealed the most consistent decrease (by almost 50 %) was registered after 12 h of treatment (Fig. 6b). No significant changes were observed in the expression levels of the 66 kDa Nrf2 form (Fig. 6a,b).

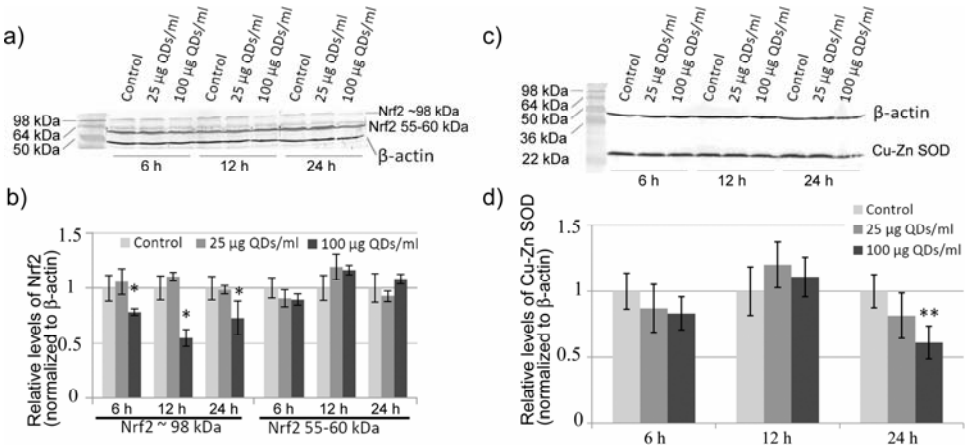

Fig. 6 – The protein expression of antioxidative transcription factor Nrf2 and cytosolic antioxidant enzyme Cu-Zn SOD. Representative immunoblots are shown for Nrf2 in a) and for Cu-Zn SOD in c). Densitometric data in b) and d) are presented as means of three independent experiments ± RSD and are expressed as ratios from corresponding controls.
Statistical significance was calculated by student T test and indicated as: *p < 0.05, ** p < 0.01.

In our experimental conditions, the decrease of Nrf2 probably affected the expression level of Cu-Zn SOD enzyme, which was significantly decreased after 24 h exposure to 100 μg/ml QDs (Fig. 6c,d). Diminished Cu-Zn SOD expression and function is known to be associated with cell death *via* an apoptotic mechanism [28–29]. The reduced cell viability observed at the 100, 200 and 300 μg/ml QDs exposure (Fig. 1) could be explained, at least partially, by apoptosis. Amorphous silicon nanoparticles ~14 nm in diameter were shown to induce apoptosis in HepG2 cells in other studies [30]. In the respective study, a 200 μg/ml nanoparticle dose was applied for 72 h, and it was found that a very similar reduction of viability as the one noticed by us after 48 h exposure to 200 μg/ml QDs occured. It seems that the smaller size of the QDs and the crystalline silicon core they contain did not contribute to increase their toxicity compared to the amorphous silicon nanoparticles. This was expected, considering the QDs are prone to aggregate in clusters and that their surface was allowed to completely oxidize [18, 20].

We propose that the QDs we used also had an antiproliferative effect, as suggested in a study using the same experimental model exposed to silicon nanoparticles [31]. In our case, the antiproliferative effect was most probably induced by the actin cytoskeleton disorganization, which probably reduced cell adherence, weakened intercellular junctions and inhibited cell division.

In a living organism, an unbalanced pro-inflammatory response may be the source of more damage than the QDs might cause alone. The capacity of Si/SiO_2 QDs to generate a pro-inflammatory response was tested through the expression and secretion of a panel of eight cytokines: IL-2, IL-4, IL-6, IL-8, IL-10, GM-CSF, IFN-γ and TNF-α. In our case, only the levels of IL-8 were detectable, both intracellular and in the cell medium (Table 1). The expression of the pro-inflammatory marker IL-8 was significantly increased under 100 μg/ml QDs both in the cell lysate and cell medium, at all the exposure intervals tested.

Table 1

IL-8 cytokine in HepG2 lysate and culture medium after exposure to Si/SiO_2 QDs

Time	6 h			12 h			24 h		
QDs dose (μg/ml)	Control	25	100	Control	25	100	Control	25	100
Intracellular IL-8 (pg/mg)	168 ± 54	216 ± 64	303 ± 61	122 ± 25	144 ± 33	245 ± 25	130 ± 25	156 ± 44	281 ± 31
Fold change	***1***	***1.29***	***1.8****	***1***	***1.18***	***2.01****	***1***	***1.2***	***2.16****
Extracellular IL-8 (pg/mg)	90 ± 7	154 ± 50	180 ± 26	169 ± 10	353 ± 19	329 ± 21	288 ± 32	375 ± 72	621 ± 42
Fold change	***1***	***1.7***	***2****	***1***	***2.09*****	***1.95*****	***1***	***1.3***	***2.16****

*p<0.05; **p < 0.01; ***p<0.001.

IL-8 increased levels were described after exposure of human monocytes to amorphous silica nanoparticles [32–33]. To our knowledge, the immunostimulatory effects of silicon QDs was not previousley characterised. IL-8 is a very potent

neutrophil chemoattractant [34] and it prepares the immune cells for the respiratory burst [35]. In our case, the inflammatory conditions were induced very early in the QDs exposed hepatocyte cells.

4. CONCLUSIONS

Our data indicated that HepG2 cells exposed to relative high doses of Si/SiO_2 QDs do not suffer significant damage, the QDs being highly compatible with this particular cell type. The moderate elevated IL-8 citokine levels, which could indicate inflammatory effects might occur in the case of an *in vivo* QDs exposure.

Acknowledgements. This work was supported by the strategic grant POSDRU/159/1.5/S/133391, Project "Doctoral and Post-doctoral programs of excellence for highly qualified human resources training for research in the field of Life Sciences, Environment and Earth Science" co-financed by the European Social Found within the sectorial Operational Program Human Resources Development 2007-2013 and by the LAPLAS 3 PN 09 39 01 05 Project.

REFERENCES

1. T. Tsuzuki, Int. J. Nanotechnol., **6**, 567–578 (2009).
2. R.J. Aitken, K.S. Creely, C.L. Tran, *Nanoparticles: An occupational hygiene review*, Edinburgh, United Kingdom, 2004.
3. X. Michalet, F.F. Pinaud, L.A. Bentolila, J.M. Tsay, S. Doose, J.J. Li, G. Sundaresan, A.M. Wu, S.S. Gambhir, S.Weiss, Science, **307**, 538–544 (2005).
4. I.L. Medintz, M.H. Stewart, S.A. Trammell, K. Susumu, J.B. Delehanty, B.C. Mei, J.S. Melinger, J.B. Blanco-Canosa, P.E. Dawson, H. Mattoussi, Nat. Mater., **9**, 676–684 (2010).
5. A.M. Derfus, W.C.W. Chan, S.N. Bhatia, Nano Lett., **4**, 11–18 (2004).
6. H. Zhang, D. Yee, C. Wang, Nanomed., **3**, 83–91 (2008).
7. S.T. Selvan, T.T. Tan, J.Y. Ying, Adv. Mater., **17**, 1620–1625 (2005).
8. S. Veeranarayanan, A.C. Poulose, M. S. Mohamed, Y. Nagaoka, S. Iwai, Y. Nakagame, S. Kashiwada, Y. Yoshida, T. Maekawa, D. S. Kumar, Int. J. Nanomed., **7**, 3769–3786 (2012).
9. N. O'Farrell, A. Houlton, B.R. Horrocks, Int. J. Nanomed. **1**, 451–472 (2006).
10. J.H. Park, L. Gu, G. Von Maltzahn, E. Ruoslahti, S.N. Bhatia, M.J. Sailor, Nat. Mater., **8**, 331–336 (2009).
11. J.K. Klostranec, W.C. Chen, Adv. Mater., **18**, 1953–1964 (2006).
12. A. Nel, T. Xia, L. Mädler, N. Li, Science, **311**, 622–627 (2006).
13. D. Napierska, L.C.J. Thomassen, D. Lison, J.A. Martens, P.H. Hoet, Partic. Fibre Toxicol., **7**:39 (2010).
14. F. Wang, F. Gao, M. Lan, H. Yuan, Y. Huang, J. Liu, Toxicol., In Vitro, **23**, 808–815 (2009).
15. D. Napierska, L.C. Thomassen, V. Rabolli, D. Lison, L., Gonzalez, M. Kirsch-Volders, J.A. Martens, P.H. Hoet, Small, **5**, 846–853 (2009).
16. Y. Ye, J. Liu, M. Chen, L. Sun, M. Lan, Environ. Toxicol. Pharmacol., **29**, 131–137 (2010).
17. F. Marano, S. Hussain, F. Rodrigues-Lima, A. Baeza-Squiban, S. Boland, Arch. Toxicol., **85**, 733–741 (2011).
18. C. Grigoriu, I. Nicolae, V. Ciupina, G. Prodan, H. Suematsu, K. Yatsui, J. Optoelectr. Adv. Mat., **6**, 825–830 (2004).
19. M.S. Stan, I. Memet, C. Sima, T. Popescu, V.S. Teodorescu, A. Hermenean, A. Dinischiotu, Chem. Biol. Interact., **220**, 102–115 (2014).

20. C. Grigoriu, Y. Kuroki, I. Nicolae, X. Zhu, M. Hirai, H. Suematsu, M. Takata, K. Yatsui, J. Optoelectr. Adv. Mat., **7**, 2979–2984 (2005).
21. M. Bradford, Anal. Biochem., **72**, 248–254 (1976).
22. J. Mosmann, J. Immunol. Methods, **65**, 55–63 (1983).
23. S.J.H. Soenen, N. Nuytten, S.F. De Meyer, S.C. De Smedt, M. De Cuyper, Small, **6**, 832–842 (2010).
24. S.J. Soenen, B. Manshian, J.M. Montenegro, F. Amin, B. Meermann, T. Thiron, M. Cornelissen, F. Vanhaecke, S. Doak, W. J. Parak, S. De Smedt, K. Braeckmans, ACS Nano, **6**, 5767–5783 (2012).
25. Y. Huang, C. Wu, R. Aronstam, Materials, **3**, 4842–4859 (2010).
26. N. Li, T. Xia, A.E. Nel, Free Radic. Biol. Med., **44**, 1689–1699 (2008).
27. J. Pi, Y. Bai, J.M. Reece, J. Williams, D. Liu, M.L. Freeman, W.E. Fahl, D. Shugar, J. Liu, W. Qu, S. Collins, M.P. Waalkes, Free Radic. Biol. Med., **42**, 1797–1806 (2007).
28. J.D. Rothstein, L.A. Bristol, B. Hosler, Jr. RH. Brown Proc. Natl. Acad. Sci., U.S.A., **91**, 4155–4159 (1994).
29. C.M. Troy, M.L. Shelanski, Proc. Natl. Acad. Sci., U.S.A., **91**, 6384–6387 (1994).
30. J. Ahmad, M. Ahamed, M.J. Akhtar, S.A. Alrokayan, M.A. Siddiqui, J. Musarrat, A.A. Al-Khedhairy, Toxicol. Appl. Pharmacol., **259**, 160–168 (2012).
31. X. Lu, J. Qian, H. Zhou, Q. Gan, W. Tang, J. Lu, Y. Yuan, C. Liu, Int. J. Nanomed., **6**, 1889–1901 (2011).
32. E.-J. Yang, I.-H. Choi, Immune Netw., **13**, 94–101 (2013).
33. D.M. Gonçalves, S. Chiasson, D. Girard, Toxicol., in Vitro, **24**, 1002–1008 (2010).
34. C. Janeway, K.P. Murphy, P. Travers, M. Walport., *Janeway's immuno biology*, Garland Science, New York, 2008.
35. C. Guichard, E. Pedruzzi, C. Dewas, M. Fay, C. Pouzet, M. Bens, A. Vandewalle, E. Ogier-Denis, M.A. Gougerot-Pocidalo, C. Elbim, J. Biol. Chem., **280**, 37021–37032 (2005).